Supporting Information of

Boosting lithium-ion battery performance: the role of a novel carbonate-based ionic liquid electrolyte additive

Boyun Wang‡[a,b,c], Na Ju‡[b], Zhigang Zhang[a,c], Dongxiang Li[a,c], Chen Yang[a,c], Suyan Niu[b], You Fu[b], Wenlong Zhang[b], Zilong Liu[b], Lei Shi[a,c], Guangwen Xu*[a,c], Hongbin Sun*[a,b]*

a Key Laboratory on Resources Chemicals and Materials of Ministry of Education, Shenyang University of Chemical Technology, Shenyang 110142, People's Republic of China.

b Department of Chemistry, Northeastern University, Shenyang 110819, People's Republic of China.

c Institute of Industrial Chemistry and Energy Technology, Shenyang University of Chemical Technology, Shenyang 110142, People's Republic of China.

Experimental

Electrolyte Preparation Methods

Synthesis of MI-EC: A mixture of 0.17 mol dehydrated ethylene carbonate (EC), 0.17 mol 1-methylimidazole, and 30 mL acetonitrile was added to a three-neck flask and stirred at 70 °C for 24 h. After the reaction, the solvent was removed by rotary evaporation, and the crude product was further purified by extraction using a mixed solvent of petroleum ether: ethyl acetate: acetone (4:2:1, v/v) to remove unreacted starting materials. Finally, the product was vacuum-dried at 85 °C for 12 h and stored in an argon-filled glovebox for subsequent electrolyte preparation. A predetermined amount of MI-EC was dissolved in the BE to obtain modified electrolytes with mass fractions of 0.5, 1.0, and 2.0 wt%, designated as ME-5, ME-10, and ME-20, respectively.

Materials

The standard electrolyte (1 M $LiPF_6$ in EC:DEC (1:1 v/v) + 2% VC, denoted as BE) was purchased from Shanghai Songjing New Energy Technology Co., Ltd. Graphite, acetylene black, and polyvinylidene fluoride (PVDF) were obtained from Guangdong Canrd New Energy Technology Co., Ltd. N-Methyl-2-pyrrolidone (NMP), ethylene carbonate, and lithium iron phosphate (LFP) were sourced from Aladdin Reagent Co., Ltd. (China). 1-Methylimidazole was procured from Shanghai Macklin Biochemical Technology Co., Ltd. Acetonitrile, petroleum ether, and ethyl acetate (EA) were supplied by Tianjin Fuyu Fine Chemical Co., Ltd. Acetone was purchased from Tianjin Damao Chemical Reagent Factory. All chemicals were of analytical grade and used as received without further purification. CR2025 coin cell kits were acquired from Dongguan Canrd New Energy Technology Co., Ltd.

Electrode Preparation and Battery Assembly

LFP Cathode Preparation: The LFP cathode was prepared by mixing active material (LFP), conductive carbon (acetylene black), and binder (PVDF) at a weight ratio of 8:1:1 in N-methyl-2-

pyrrolidone (NMP) to form a homogeneous slurry. The mixture was coated onto an aluminum foil current collector, dried at 80 °C to remove the solvent, and further vacuum-dried for 12 h. The dried electrode was then cut into discs with a diameter of 14 mm. The mass loading of the active material was approximately 3.8 mg cm^{-2}.

Graphite Anode Preparation: The graphite anode was prepared following the same procedure as described above. The mass loading of the active material was approximately 2.0 mg cm^{-2}

Coin cells assembly was conducted in an argon-filled glovebox with both moisture (H_2O) and oxygen (O_2) levels maintained below 0.1 ppm.

The Li||Li symmetric CR2032 cells were assembled by stacking two lithium metal electrodes with a polyethylene (PE) separator**.** LFP||Li half-cell consisted of an LFP cathode, a PE separator, and a lithium metal anode. Graphite||Li half-cell was constructed using a graphite anode, a PE separator, and a lithium metal counter electrode. LFP||graphite full cell was fabricated by pairing an LFP cathode with a graphite anode, separated by a PE membrane.

Performance Testing

Constant current charging was performed at a current density of 1 mA cm^{-2} for the lithium deposition test to observe the formation of lithium deposits in the in-situ cell. Galvanostatic charge-discharge tests and rate capability tests were conducted using a multi-channel battery testing system (LAND, CT3002A). Tafel tests, cyclic voltammetry (CV), and electrochemical impedance spectroscopy (EIS) measurements were performed on a CHI660E electrochemical workstation (Chenhua, China). Steady-state polarization tests for Li||Li symmetric cells were carried out on the CHI660E electrochemical workstation, applying a bias voltage of 10 mV for a polarization duration of 0.5 hours. The lithium-ion transference number (t_{Li^+}) was calculated using the Bruce-Vincent-Evans equation:

$$t_{Li^+} = \frac{I_{ss} \times (\Delta V - I_0 \times R_0)}{I_0 \times (\Delta V - I_{ss} \times R_{ss})}$$

where ΔV is the applied voltage, I_0 and I_{ss} represent the initial and steady-state currents, respectively, and R_0 and R_{ss} denote the resistances before and after polarization.

The ionic conductivity was calculated from the EIS data of a SS||SS coin cell (SS stands for the stainless steel plate). The conductivity of electrolyte was obtained by the following equation:

$$\sigma = \frac{L}{R \times S}$$

In this equation, σ is the conductivity of electrolyte, L is the length of the testing cell, S stands for the contact area between the electrode and electrolyte in the testing cell and R represents the charge resistance.

Characterization

^{1}H nuclear magnetic resonance (NMR) spectroscopy was performed on a Bruker AVANCE III 500 MHz spectrometer. The surface morphology of cycled electrodes was examined using scanning electron microscopy (SEM, JSM-IT800), transmission electron microscopy (TEM, JEOL), and atomic force microscopy (AFM, Bruker Dimension Icon). The chemical composition of the electrode surfaces was characterized by X-ray photoelectron spectroscopy (XPS, Axis Supra+).

Quantum chemistry calculations

Density functional theory (DFT) calculations were performed using the Gaussian 16 software package [1]. Geometry optimizations and frequency analyses were carried out at the B3LYP level of theory with the 6-31G(d) basis set[2-4]. Grimme's D3 dispersion correction with Becke-Johnson damping (GD3BJ) was employed to account for long-range dispersion interactions. To further analyze the nature of the interactions, wavefunction analysis was performed using the Multiwfn

program, and molecular visualizations were generated with Visual Molecular Dynamics (VMD)[5, 6].

Molecular dynamics (MD) simulations

MD simulations for the electrolyte structures were conducted by using the GROMACS package with Amber force fields[7, 8]. The size of box is 5 × 5 × 5 nm^3, and periodic boundary conditions were set in all three directions. The electrostatic interactions were computed using PME methods. A cutoff length of 1.0 nm was used in the calculation of electrostatic interactions and non-electrostatic interactions in real space. The integration time step was 1 fs. The system was annealed from 298.15 to 398.15 K over a period of 1 ns. After reaching quasi-equilibrium, each electrolyte system underwent a total of 100 ns of MD simulation. Initially, a 40 ns NVT ensemble simulation at 398.15 K was performed, followed by a 40 ns NPT ensemble run at 298.15 K to achieve thermal and pressure equilibration. Subsequently, a 20 ns NPT simulation was carried out to evaluate radial distribution functions and coordination numbers across different electrolyte systems. The simulation snapshots were visualized using VMD software[5].

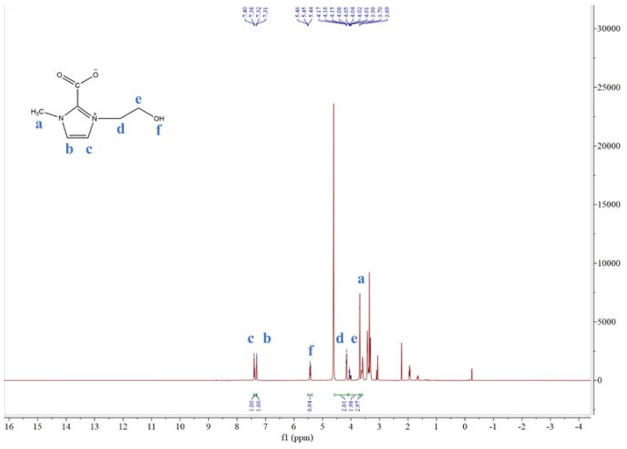

Figure S1. ^{1}H NMR spectrum of MI-EC.

The NMR characterization results are as follows: ^{1}H NMR (500 MHz, Methanol-d$_4$) δ 7.39 (d, J = 13.2 Hz, 1H), 7.31 (d, J = 6.1 Hz, 1H), 5.45 (t, *J* = 7.9 Hz, 1H), 4.58-4.10 (m, 2H), 4.08-3.69 (m, 2H), 3.69 (s, 3H).

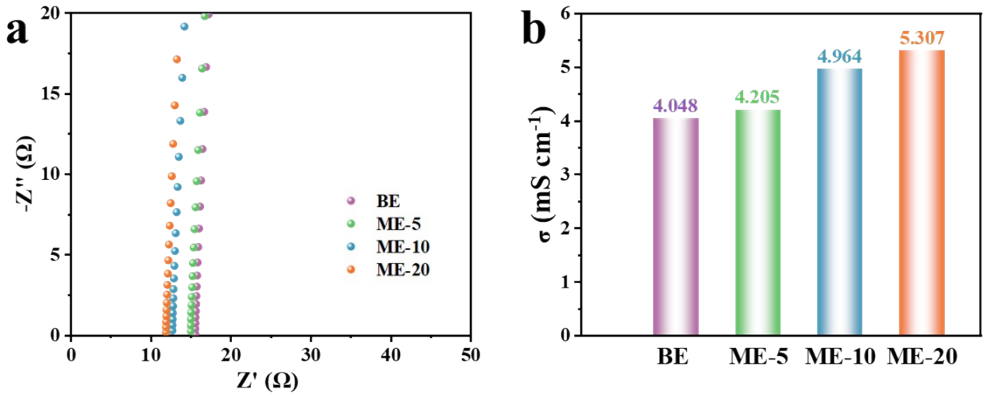

Figure S2. Comparison of ionic conductivity of different electrolytes.

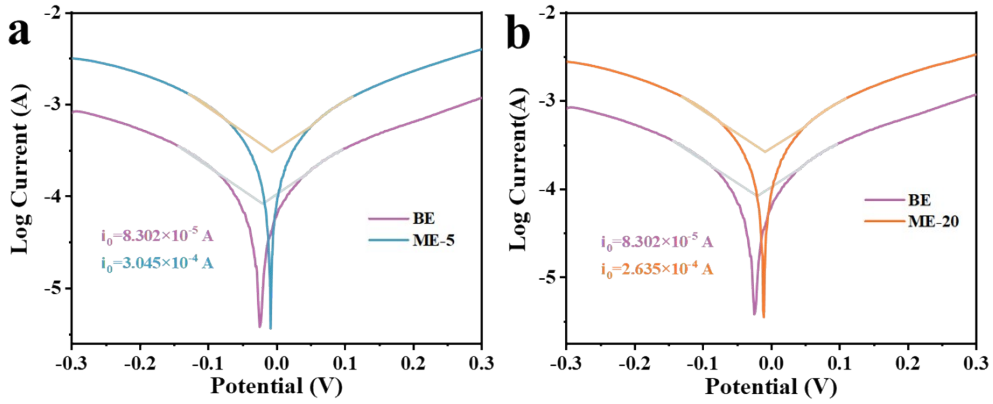

Figure S3. Tafel plots of Li||Li symmetric cells within the voltage range of -0.3 to 0.3 V.

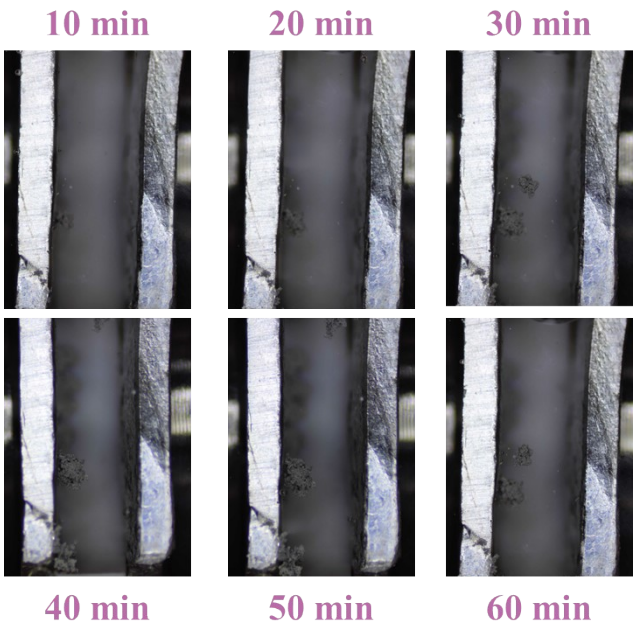

Figure S4. In-situ optical images of lithium deposition at 10 - 60 min in BE.

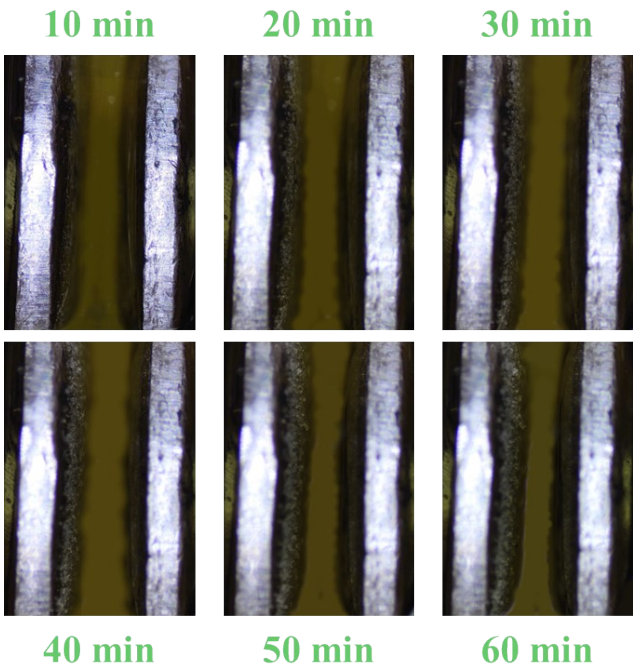

Figure S5. In-situ optical images of lithium deposition at 10 - 60 min in ME-10 electrolyte.

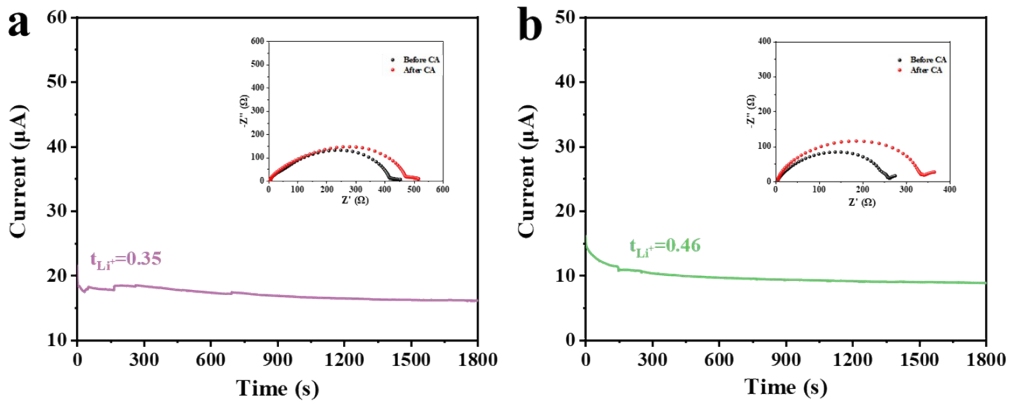

Figure S6. Lithium-ion transference numbers for (a) BE and (b) ME-10 electrolytes, measured using Li||Li symmetric cells under polarization. The inset shows the electrochemical impedance spectra of the symmetric cell before and after polarization.

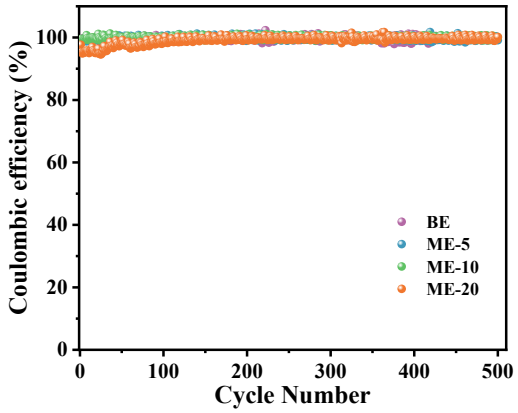

Figure S7. Coulombic efficiency of LFP||Li half-cells during long-term cycling at 0.5 C in different electrolytes.

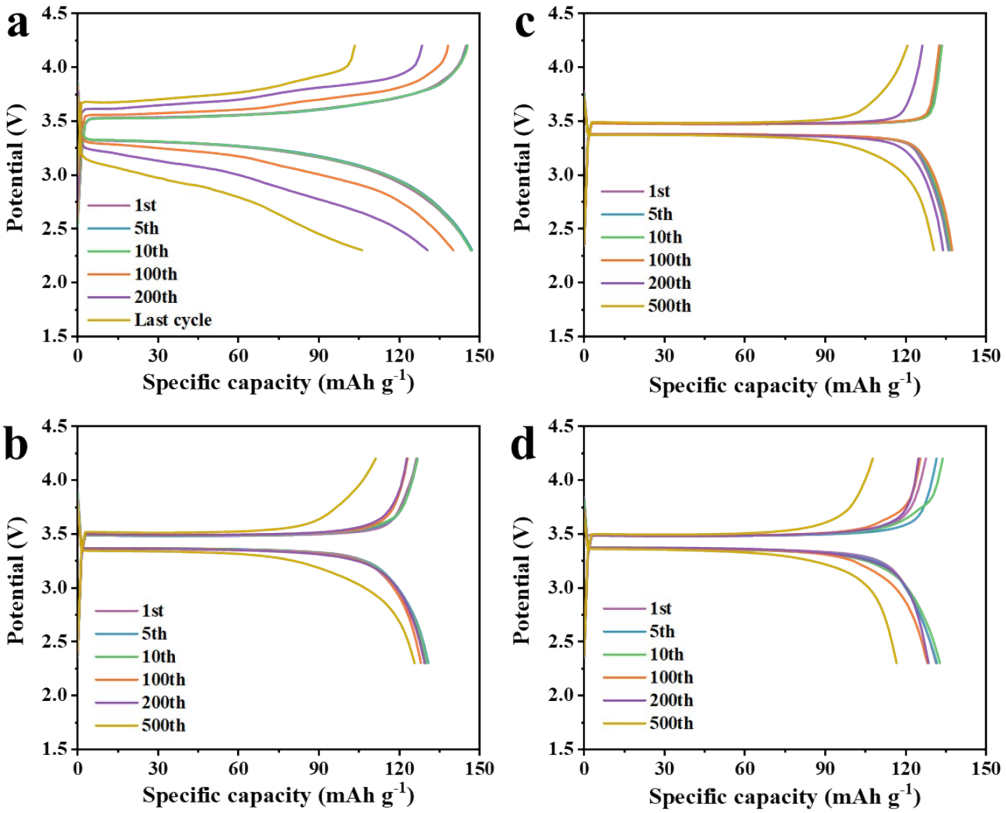

Figure S8. GCD curves of LFP||Li half-cells during long-term cycling at 0.5 C in (a) BE, (b) ME-5, (c) ME-10, and (d) ME-20 electrolytes.

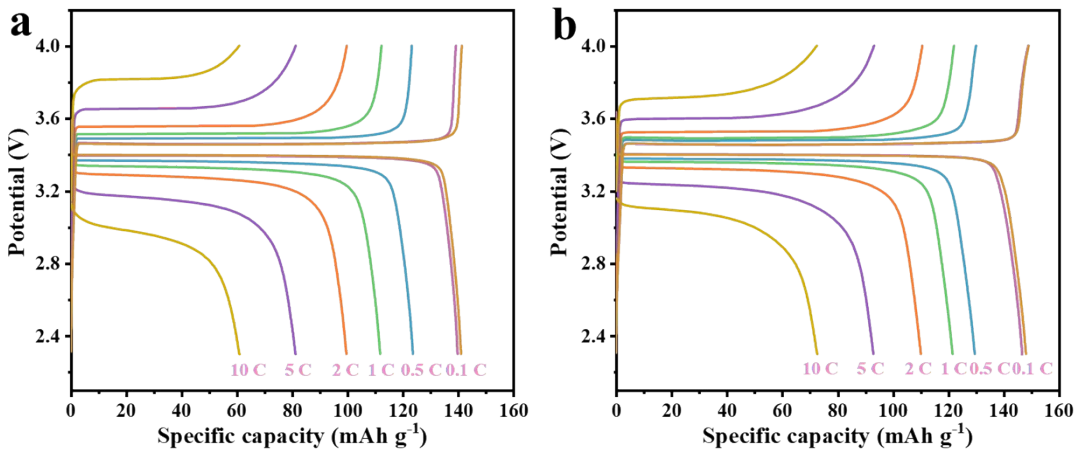

Figure S9. GCD curves of LFP half-cells at different current densities in (a) BE and (b) ME-10 electrolytes.

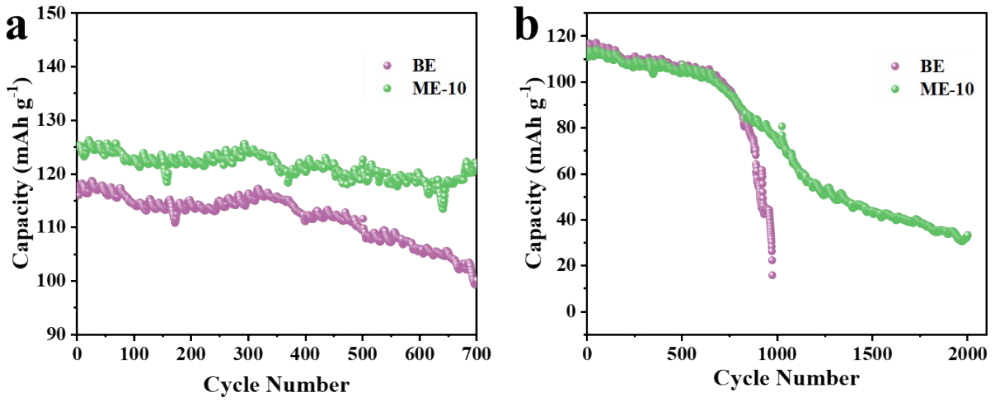

Figure S10. Long-term cycling performance of LFP half-cells at (a) 1 C and (b) 2 C rates in different electrolytes.

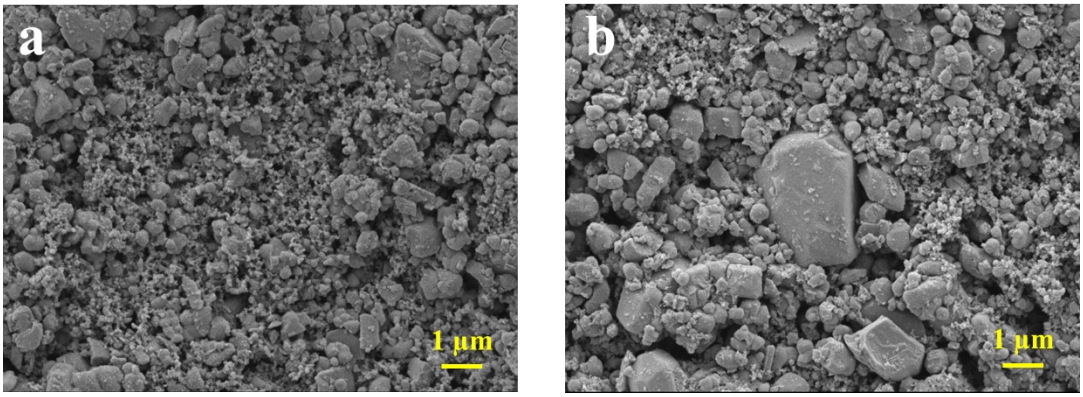

Figure S11. SEM images of LFP cathodes after 100 cycles at 1 C in different electrolytes: (a) cycled in BE; (d) cycled in ME-10 (scale bar: 1 µm).

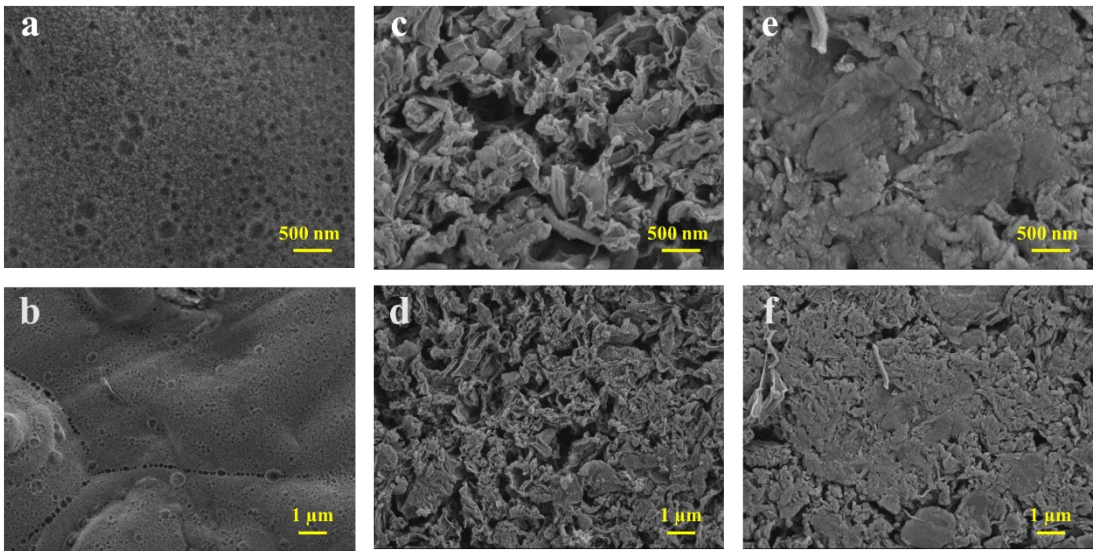

Figure S12. (a, b) Pristine lithium metal surface; SEM images of lithium anodes after 100 cycles at 1 C in LFP half-cells with different electrolytes: (c, d) cycled in BE; (e, f) cycled in ME-10.

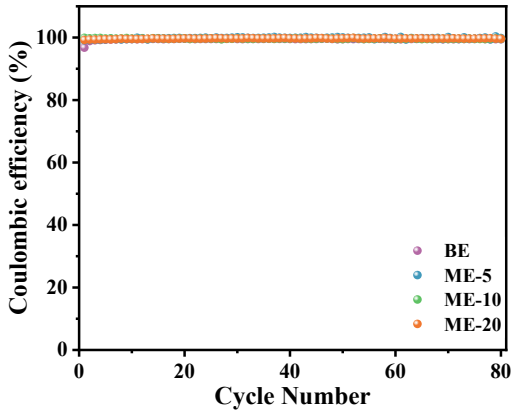

Figure S13. Coulombic efficiency of graphite half-cells during long-term cycling at 0.5 C in different electrolytes.

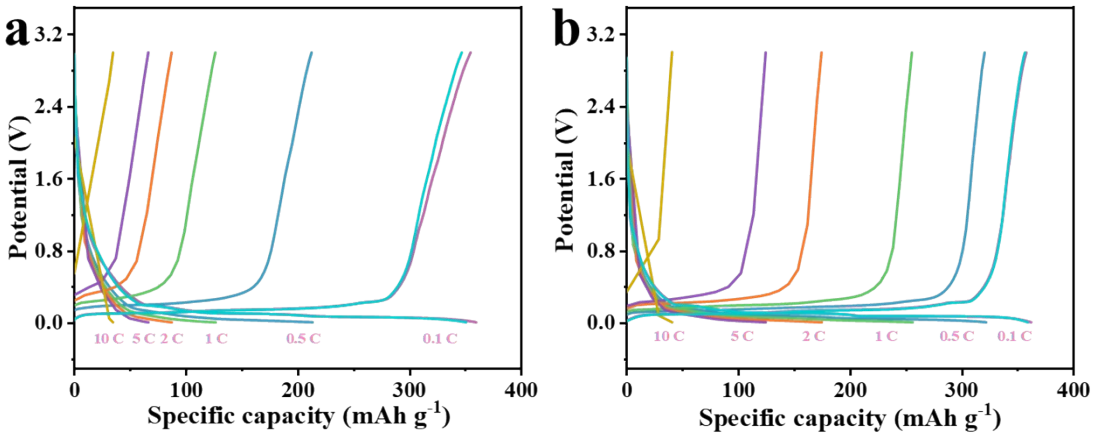

Figure S14. GCD curves of graphite half-cells at different current densities in (a) BE and (b) ME-10 electrolytes.

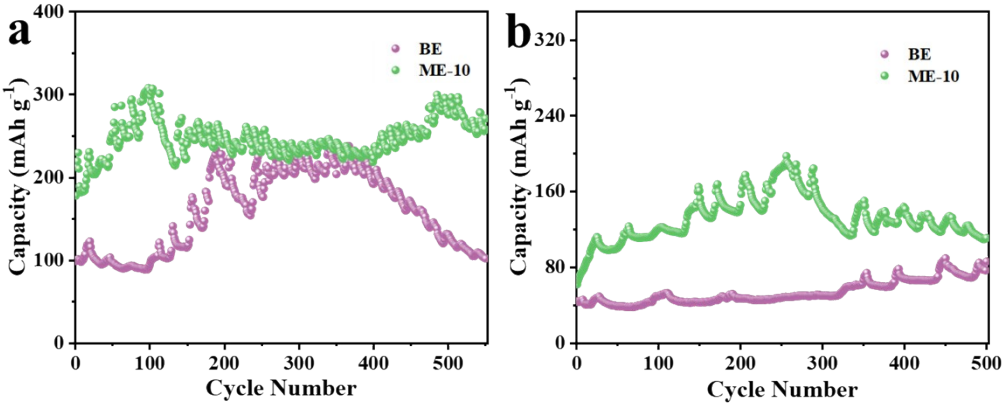

Figure S15. Long-term cycling performance of graphite half-cells at (a) 1 C and (b) 2 C rates.

The initial capacity increase observed in the BE electrolyte during cycling may be attributed to temperature variations.

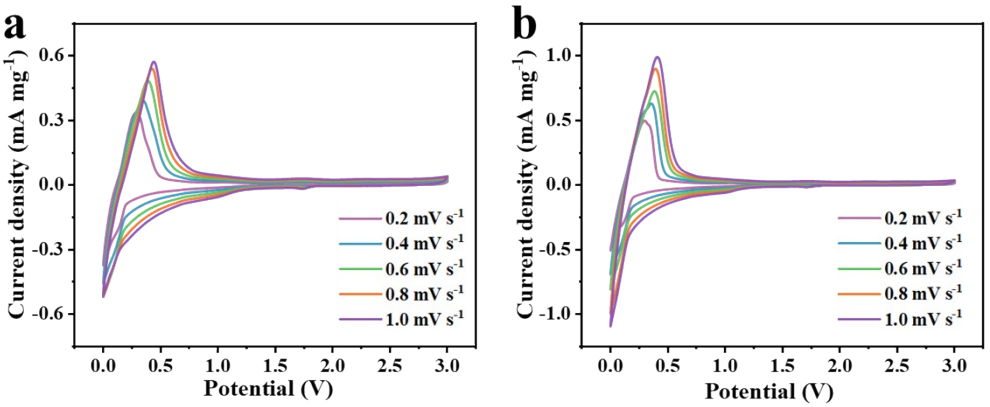

Figure S16. CV profiles of graphite||Li half-cells: CV curves from 0.2 to 1.0 mV s^{-1} in (a) BE and (b) ME-10 electrolytes.

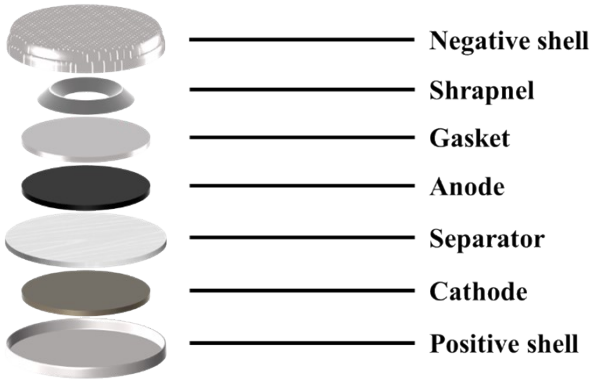

Figure S17. Schematic illustration of the assembled LFP||graphite full cell.

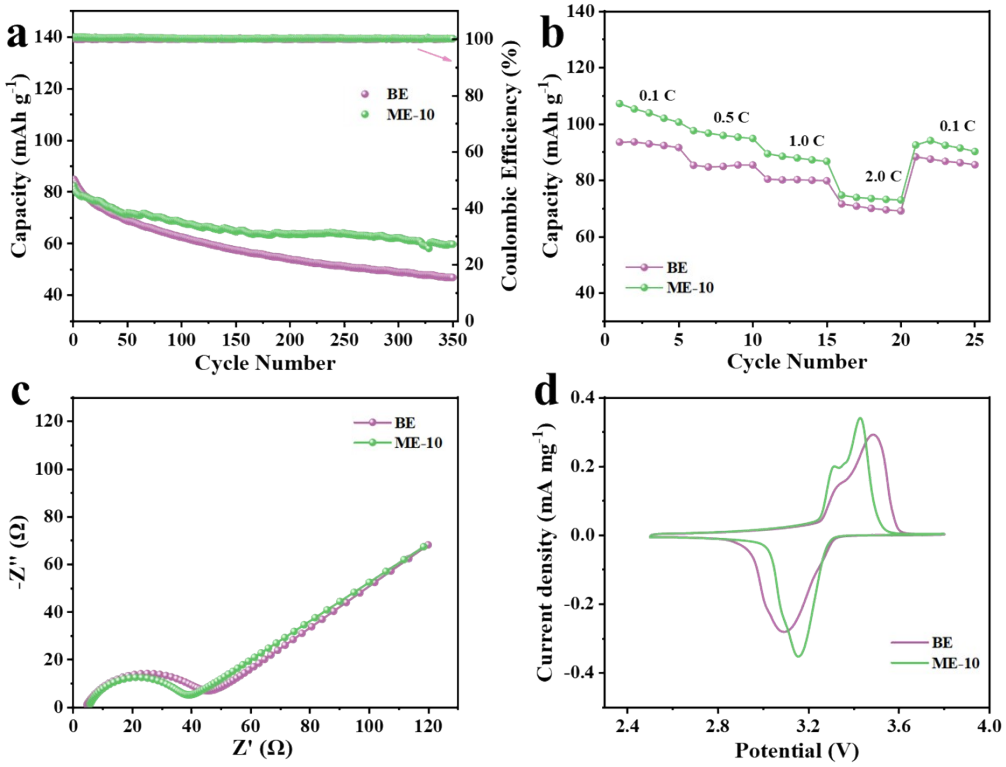

Figure S18. Electrochemical performance of LFP||graphite full cells: (a) GCD curves at 0.5 C in different electrolytes; (b) Rate capability; (c) EIS spectra after 3 cycles at 0.1 C; (d) CV curves at a scan rate of 0.2 mV s^{-1}.

Table S1. Coordination numbers of Li^+ in BE and ME-10 electrolytes obtained from MD simulations.

	Li-O(MI-EC)	Li-O(EC)	Li-O(VC)	Li-O(DEC)	Li-F(PF_6^-)
BE		0.877	0.634	0.505	1.635
ME-10	5.205	0.168	0.45	1.435	0.817

Table S2. Voltage polarization derived from the GCD curves of the LFP||Li half-cell during the last cycle of the 0.5 C long-term cycling test.

	BE	ME-5	ME-10	ME-20
Charge Voltage/V	3.74	3.52	3.48	3.51
Discharge Voltage/V	2.86	3.31	3.35	3.33
ΔV	0.88	0.21	0.13	0.18

Table S3. Peak area and relative percentage of XPS spectra for the LFP electrode in BE.

	C 1s				O 1s		F 1s		N 1s	
Peak	C-C	C-O	C=O	O-C=O	C=O	C-O	Li-F	C-F	C-N	C=N
Area	38495.2	24581.21	5833.39	8603.58	62882.54	53682.72	75365.3	80843.67	1216.22	
Peak Percentage	0.50	0.32	0.08	0.11	0.54	0.46	0.48	0.52	1.00	

Table S4. Peak area and relative percentage of XPS spectra for the LFP electrode in ME-10 electrolyte.

	C 1s				O 1s		F 1s		N 1s	
Peak	C-C	C-O	C=O	O-C=O	C=O	C-O	Li-F	C-F	C-N	C=N
Area	22237.79	34138.92	5044.42	8187.59	43913.22	41603.04	121534.58	75541.66	3575.42	1530.46
Peak Percentage	0.32	0.49	0.07	0.12	0.51	0.49	0.62	0.38	0.70	0.30

Table S5. Peak area and relative percentage of XPS spectra for the C electrode in BE.

	C 1s				O 1s		N 1s	
Peak	C-C	C-O	C=O	O-C=O	C=O	C-O	C-N	C=N
Area	15706.24	9180.56	4372.85	3677.11	73792.24	22214.81	872.16	
Peak Percentage	0.48	0.28	0.13	0.11	0.77	0.23	1.00	

Table S6. Peak area and relative percentage of XPS spectra for the graphite electrode in ME-10 electrolyte.

	C 1s				O 1s		N 1s	
Peak	C-C	C-O	C=O	O-C=O	C=O	C-O	C-N	C=N
Area	35638.26	12641.88	3147.08	21962.7	163181.5	32004.26	974.57	478.48
Peak Percentage	0.49	0.17	0.04	0.30	0.84	0.16	0.67	0.33

REFERENCES

1 M. J. Frisch, G. W. Trucks, H. B. Schlegel, G. E. Scuseria, M. A. Robb, J. R. Cheeseman, G. Scalmani, V. Barone, G. A. Petersson, H. Nakatsuji, X. Li, M. Caricato, A. V. Marenich, J. Bloino, B. G. Janesko, R. Gomperts, B. Mennucci, H. P. Hratchian, J. V. Ortiz, A. F. Izmaylov, J. L. Sonnenberg, Williams, F. Ding, F. Lipparini, F. Egidi, J. Goings, B. Peng, A. Petrone, T. Henderson, D. Ranasinghe, V. G. Zakrzewski, J. Gao, N. Rega, G. Zheng, W. Liang, M. Hada, M. Ehara, K. Toyota, R. Fukuda, J. Hasegawa, M. Ishida, T. Nakajima, Y. Honda, O. Kitao, H. Nakai, T. Vreven, K. Throssell, J. A. Montgomery Jr., J. E. Peralta, F. Ogliaro, M. J. Bearpark, J. J. Heyd, E. N. Brothers, K. N. Kudin, V. N. Staroverov, T. A. Keith, R. Kobayashi, J. Normand, K. Raghavachari, A. P. Rendell, J. C. Burant, S. S. Iyengar, J. Tomasi, M. Cossi, J. M. Millam, M. Klene, C. Adamo, R. Cammi, J. W. Ochterski, R. L. Martin, K. Morokuma, O. Farkas, J. B. Foresman and D. J. Fox, *Journal*, 2016.

2 T. Yanai, D. P. Tew and N. C. Handy, *Chemical Physics Letters*, 2004, **393**, 51-57.

3 P. J. Stephens, F. J. Devlin, C. F. Chabalowski and M. J. Frisch, *The Journal of Physical Chemistry*, 1994, **98**, 11623-11627.

4 M. P. Andersson and P. Uvdal, *The Journal of Physical Chemistry A*, 2005, **109**, 2937-2941.

5 T. Lu and F. Chen, *Journal of Computational Chemistry*, 2012, **33**, 580-592.

6 W. Humphrey, A. Dalke and K. Schulten, *Journal of Molecular Graphics*, 1996, **14**, 33-38.

7 C. K. Berk Hess, David van der Spoel, Erik Lindahl, *J. Chem*, 2008, **4**, 435-447.

8 E. Lindahl, B. Hess and D. van der Spoel, *Journal of Molecular Modeling*, 2001, **7**, 306-317.